DOI:10.1093/jnci/djs224
Advance Access publication on May 3, 2012.

ARTICLE

Role of the Tripartite Motif Protein 27 in Cancer Development

Georgia Zoumpoulidou, Cristina Broceño, He Li, Demelza Bird, George Thomas, Sibylle Mittnacht

Manuscript received August 10, 2011; revised March 28, 2012; accepted March 29, 2012.

Correspondence to: Georgia Zoumpoulidou, BSc (hons), MSc, PhD, Section of Cancer Biology, University College London Cancer Institute, University College London, 72 Huntley St, London WC1E 6DD, UK (e-mail: g.zoumpoulidou@cancer.ucl.ac.uk) and Sibylle Mittnacht, MPhil, PhD, Section of Cancer Biology, University College London Cancer Institute, University College London, 72 Huntley St, London WC1E 6DD, UK (e-mail: s.mittnacht@cancer.ucl.ac.uk).

Background The tripartite motif family protein 27 (TRIM27) is a transcriptional repressor that interacts with, and attenuates senescence induction by, the retinoblastoma-associated protein (RB1). High expression of TRIM27 was noted in several human cancer types including breast and endometrial cancer, where elevated TRIM27 expression predicts poor prognosis. Here, we investigated the role of TRIM27 expression in cancer development.

Methods We assessed TRIM27 expression in human cancer using cancer profiling arrays containing paired tumor and normal cRNA (n = 261) as well as in murine skin cancer induced by 7, 12-dimethylbenzanthracene (DMBA)/12-O-tetradecanoylphorbol-13-acetate (TPA). We generated mice with disrupted expression of murine TRIM27 ($Trim27^{-/-}$) and assessed their susceptibility to DMBA/TPA-induced skin tumor development compared with isogenic littermates (n = 26 mice per group). We assessed the effect of Trim27 loss on senescence propensity in mouse embryonic fibroblasts (MEFs) by quantifying cell proliferation alongside senescence markers (senescence-associated β-galactosidase [SA-β-gal] activity and hypertrophic cell morphology). The contribution of RB1 on senescence and cancer susceptibility (n > 20 mice per group) in $Trim27^{-/-}$ backgrounds was also assessed. Data were analyzed using the Student's *t*, χ^2, or log-rank test as indicated. All statistical tests were two-sided.

Results TRIM27 transcript levels are statistically significantly increased in common human cancers, including colon and lung, vs normal tissues (TRIM27 expression relative to ubiquitin: cancers vs normal tissues, mean = 0.59, 95% confidence interval [CI] = 0.55 to 0.63 vs mean = 0.46, 95% CI =0.43 to 0.49, $P < .001$) as well as in chemically induced mouse skin cancer compared with matched normal tissue (Trim27 expression relative to Gapdh control: tumor vs normal skin, mean = 4.2, 95% CI = 3.97 to 4.43 vs mean = 0.96, 95% CI = 0.69 to 1.2, $P < .001$). $Trim27^{-/-}$ mice (n = 14) were resistant to chemically induced skin cancer development (eight [57.2%] of 14 mice were tumor free) compared with $Trim27^{+/+}$ wild-type littermates (n = 13) (one [7.7%] of 13 mice was tumor free). $Trim27^{-/-}$ MEFs show enhanced senescence propensity in response to replicative (percentage of SA-β-gal-positive cells: $Trim27^{+/+}$ MEFs vs $Trim27^{-/-}$ MEFs, mean = 14.2%, 95% CI = 11.1% to 17.4% vs mean = 53.3%, 95% CI = 48.7% to 57.9%, $P < .001$) or oncogenic stress (percentage of SA-β-gal-positive cells: $Trim27^{+/+}$ MEFs + Ras vs $Trim27^{-/-}$ MEFs + Ras, mean = 24.0%, 95% CI = 19.9% to 28.1% vs mean = 37.3%, 95% CI = 32.2% to 42.4%, $P < .05$) compared with $Trim27^{+/+}$ MEFs. These responses were alleviated following inactivation of murine RB1 (Rb1). Furthermore, $Trim27^{-/-}$ mice are not protected from cancers arising as a consequence of Rb1 deletion (median survival: $Trim27^{-/-}Rb^{+/-}$ vs $Trim27^{+/+}Rb^{+/-}$, 14 vs 13 months; difference = 1.0 month, 95% CI = 0.5 to 1.6 months, $P = .14$).

Conclusion TRIM27 expression is a modifier of disease incidence and progression relevant to the development of common human cancers and is a potential target for intervention in cancer.

J Natl Cancer Inst 2012;104:941–952

Cancers arise from epigenetic and genetic alteration. Rate-limiting accumulation of such alterations combined with natural selection leads to complex changes in cell behavior that underlie cancer development and progression (1,2). Although the number of genetic alterations involved in driving cancer development is probably larger than originally expected, many alterations found in tumors may not contribute to cancer formation, but merely be passenger or bystander alterations occurring serendipitously, or as a neutral consequence of genomic and proteomic deregulation. Distinguishing whether alterations drive cancer development or arise as passengers is critical for our understanding of the cellular processes leading to cancers as well as for the design of intervening strategies.

Tripartite motif family protein 27 (TRIM27) was previously identified as a gene involved in oncogenic rearrangements with the RET tyrosine kinase receptor (3,4). More recently, evidence has emerged that the non-rearranged allele is highly and/or ectopically

CONTEXT AND CAVEATS

Prior knowledge

Tripartite motif family protein 27 (TRIM27) has previously been implicated as having a potential role in cancer development. The mechanisms by which TRIM27 participates in cancer development are poorly understood, although previous data suggest that TRIM27 modifies the function of the retinoblastoma-associated protein (RB1) tumor suppressor in cells.

Study design

To investigate the role of TRIM27 in the development of cancer, mice with defective expression of the TRIM27 murine ortholog (Trim27) were generated. The skin of $Trim27^{-/-}$ and $Trim27^{+/+}$ wild-type mice was exposed to 7, 12-dimethylbenzanthracene (DMBA)/12-O-tetradecanoylphorbol-13-acetate (TPA), as part of a two-step carcinogenesis model, and tumor incidence was compared. In vitro studies with $Trim27^{-/-}$ and $Trim27^{+/+}$ mouse embryonic fibroblasts investigated senescence in response to replicative and oncogenic stress. The role of TRIM27 in cancers caused by the loss of murine RB1 (Rb1) was also studied using Trim27/Rb1 genetically engineered mice.

Contribution

Tumor incidence in response to carcinogen exposure among $Trim27^{-/-}$ mice was decreased compared with $Trim27^{+/+}$ wild-type littermates. Increased senescence was observed when $Trim27^{-/-}$ MEFs were exposed to replicative or oncogenic stress. The incidence of cancers driven by Rb1 loss was not altered.

Implication

Trim27 plays a role in tumor development in mice and is a potential chemopreventative and therapeutic target for humans.

Limitation

A murine skin cancer model was used vs a murine model of human cancers in which TRIM27 is overexpressed, and should be used in future studies.

From the Editors

expressed in specific cancer types, including seminomas, breast, and endometrial cancers (5–7). In endometrial cancers, TRIM27 positivity predicted unfavorable clinical outcome (6). Such evidence is consistent with a linkage of TRIM27 expression to the natural history of cancer and indicates a role for the gene and its encoded product in cancer development.

The TRIM27 protein belongs to an extended, yet poorly understood, family of proteins that feature as a common denominator a tripartite combinatorial motif encompassing RING finger, B-box, and coiled-coil domain homologies (8). Various members of this gene family are implicated in ubiquitin metabolic processes, and several have been linked to pathology of diseases, including cancer (9–12).

Current functional information indicates that TRIM27 is associated with a variety of subcellular topologies and processes. Several interactions of TRIM27 with other proteins have been reported including with the E3 SUMO protein ligase PIAS3 (13,14), several ubiquitin-conjugating enzymes (15–17), chromatin components such as enhancer of polycomb (18) and the EID-1 inhibitor of differentiation and protein acetylation (19), as well as several members of the inhibitor of nuclear factor kappa B kinases (IKKs) (20). We recently described that TRIM27 can inhibit activation of gene transcription by the product of the retinoblastoma susceptibility gene (RB1) and that its ectopic expression restrains senescence expressivity arising in cells with chronic RB1 product activity (19). Our previous data suggested that TRIM27 acts to modify the function of the RB1 tumor suppressor in cells. Here, we investigated the role of TRIM27 in cancer development using the two-stage chemical carcinogenesis in mouse skin (21).

Materials and Methods

Cancer Expression Profiling

A commercial cancer-profiling array (Clontech, BD Biosciences, Oxford, UK) with paired normal and micro-dissected cancer tissue–derived cRNA preparations was sequentially hybridized with radiolabeled cDNA representing TRIM27-α or ubiquitin as per the manufacturer's instructions. Hybridization signals were detected by phosphoimaging using a Storm 820 System for data collection and ImageQuant software (GE Healthcare, Buckinghamshire, UK) linked to Microsoft Office Excel (version 2007, licensed to University College London, London, UK) for analysis.

Generation of Trim27 Mutant Mice

XP0484 embryonic stem cells containing a gene trap insertion into exon 1 of the mouse Trim27 locus were obtained from Sanger Institute Gene Trap Resource (www.sanger.ac.uk/PostGenomics/genetrap/protocols.shtml). The site of insertion was mapped by Expand Long Template PCR System (Roche, West Sussex, UK) using Trim27 intron 1 spanning primers (forward 5′-GGGAGCCTCTGAAGCTGTACT-3′, reverse 5′-TCTTTCACTCTTCTTAG-3′). Chimeric mice were produced and backcrossed to syngeneity (n > 8, where n is equal to the number of generations) into C57BL6 backgrounds. Mouse experiments were done in accordance with protocols approved by the Institutional Review Board on animal experiments at the Institute of Cancer Research (London, UK) in line with the UK Animals (Scientific Procedures) Act of 1986. Genotyping of mice was performed using the following primers: F1: 5′-ACAAAGGAGATGCACATGGAGC-3′; R2: 5-GCCAGCAAGTGTGTTAGCAA-3′; and R3: 5′-GCTTCACTGAGTCTCTGGCAT-3′.

Cell Culture, Proliferation, and Senescence

Primary mouse embryonic fibroblasts (MEFs) were derived from individual day 13.5 embryos obtained from $Trim27^{+/-} \times Trim27^{+/-}$ crosses as previously described (22). Briefly, heads and red organs were removed, and the embryo torso was minced using a sterile scalpel. Tissue clumps were dispersed by treatment with 0.5% trypsin (Sigma, Dorset, UK) for 30 minutes at 37°C. The resulting cells suspension was mixed with Dulbecco's modified Eagle medium (Gibco, Paisley, UK) supplemented with 10% fetal bovine serum (PAA Labs, Somerset, UK) and seeded into two 25-cm^2 flasks per embryo. Cells were subcultured when confluent into a 10-cm diameter dish and incubated for 2 days. These cells were frozen in aliquots and considered passage 0 (P0). Cells were maintained in an incubator with 5% CO_2 at 37°C, 3% O_2. Analysis of a minimum of three independent MEF pairs was undertaken for

each dataset. Short-term MEF proliferation was measured by plating equal cell numbers (9×10^4 cells) from each genotype into six-well plates in triplicate. Trypsin–EDTA solution (1 mL of a 0.25% solution) (Sigma) was added to cell cultures, cells were collected, and then counted using a Scepter (PHCC20060) cell counter (Merck-Millipore, Watford, UK).

MEFs were cultured by the schedule set out in the 3T3 cultivation protocol. The protocol was carried out as previously described (23). Briefly, 3×10^5 MEF cells were plated in 25-cm^2 flasks for each genotype. After 3 days, the total number of cells in the flask was counted and 3×10^5 cells were replated for 28–30 passages. The fold cell growth was calculated by dividing the number of cells counted at each passage by the number of cells initially plated (ie, 3×10^5 cells). For the study of replicative senescence, cells were maintained in 5% CO_2 at 37°C with ambient O_2. Senescence-associated β-galactosidase (SA-β-gal) was assayed as previously described (24). Briefly, MEFs (1×10^4 cells) in six-well dishes were fixed in 0.5% glutaraldehyde (in phosphate-buffered saline [PBS]) (Sigma) for 15 minutes at room temperature and washed in PBS supplemented with 1 mM $MgCl_2$. MEFs were stained with X-gal solution (1 mg/mL X-gal [Sigma], 5 mM $K_3Fe(CN)_6$, 5 mM $K_4Fe(CN)_6$, 1 mM $MgCl_2$ in PBS at pH 6.0) overnight at 37°C and SA-β-gal positive cells quantified by scoring 2–3 eye fields (between 100–200 cells) per well.

DNA Constructs and Retroviral Infection

Oncogenic Ras (HRas V12) was transduced using a pBabe-puro-based vector (pBABE puro HRas V12) (Addgene plasmid 9051; Addgene, Cambridge, MA) or a murine stem cell virus–based vector with integral internal ribosome entry site linked to the enhanced form of green fluorescent protein (MSCV/HRas V12/RES/GFP) (Addgene plasmid 18780). pBABE-puro (Addgene plasmid 1764) or parent MSCV/IRES/GFP (Addgene plasmid 9044) were used as controls. pBabe-puro-HPV16E7 expressing human papilloma virus 16 early protein E7 was provided by Dr Karl Muenger (Harvard Medical School, Boston, MA). The generation of retroviruses and infection of cells followed standard procedures. Briefly, the retroviral vector DNA was transfected into BOSC23 or Phoenix (RVC-10001; Orbigen, San Diego, CA) packaging cells (1×10^6 cells) using Fugene HD (Roche) or calcium phosphate (Promega, Southampton, UK), using the manufacturer's instruction. Cells were maintained in Dulbecco's modified Eagle medium (Gibco) supplemented with 10% fetal bovine serum (PAA Labs) in an incubator with 5% CO_2 at 37°C. Retrovirus containing supernatants were harvested 48 and 72 hours after transfection, pooled, filtered through a 0.45-μM membrane, and mixed with polybrene (Sigma) to yield a final concentration of 4%. Viral preparations were stored at −80°C or used to infect MEFs at passage 2–4.

For retroviral infections, MEFs were plated at 1×10^6 cells per 10-cm dish 24 hours before infection. For infection, the culture medium was replaced by polybrene-containing viral supernatant, and MEFs were incubated at 37°C for 8 hours at which time a second aliquot of virus was added for a further 8 hours. After 16 hours, infected cell populations were subjected to selection for virus uptake. Cells were cultured in the presence of 2 μg/mL puromycin (Sigma) for vectors encoding puromycin resistance or subjected to fluorescent cell sorting for vectors encoding green fluorescent protein (GFP).

Quantitative Real-Time Polymerase Chain Reaction

RNA expression levels were determined by quantitative real-time polymerase chain reaction (qRT-PCR) using an ABI Prism 7700 Sequence Detection System (Applied Biosystems, Paisley, UK). Total cellular RNA was isolated with TRIzol (Invitrogen, Paisley, UK) using the manufacturer's protocol. Total RNA (1 μg) was reverse transcribed into cDNA using Superscript II RNase H Reverse Transcriptase kit (Invitrogen). Fluorogenic Taqman probes and TaqMan One-step RT-PCR master reagent were used for the qRT-PCR. Four Taqman mouse primer sets (catalog numbers Mm01136022, Mm00493339, Mm00493340, and Mm00493341; Applied Biosystems) were used to amplify Trim27. The GAPDH detection kit from Applied Biosystems was used to amplify glyceraldehyde-3-phosphate dehydrogenase (GAPDH). The qRT-PCR product values obtained for Trim27 were normalized using those obtained for GAPDH for the respective samples.

In Vivo Tumor Experiments

For the two-stage skin tumorigenesis, the dorsal skin of age-matched (8-week-old) female and male mice, generated from crossing $Trim27^{+/-}$ male and female mice in a C57BL6/DBA F1 genetic background, was shaved. The following day, 150 μL of 125 μg/mL 7, 12-dimethylbenzanthracene (DMBA) (Sigma) was topically applied to the shaved area to initiate tumor development. One week following initiation, 150 μL of 10^{-4} M 12-O-tetradecanoylphorbol-13-acetate (TPA) (Sigma) was topically applied to the same area. Application was repeated twice weekly for the duration of the experiment, up to a maximum of 20 weeks. Mice were killed by CO_2 asphyxiation if any individual tumor became ulcerated or reached a diameter of 1.5 cm, if mice showed signs of distress, or at the experiment endpoint. Tumors were excised at the experiment endpoint along with tumor-adjacent and remote normal tissue as required for the experiments. Specimens were quick-frozen in liquid nitrogen for RNA and DNA analysis and either fresh frozen in Optimal Cutting Temperature (OCT) solution (Raymond Lamb, Surrey, UK) or fixed in 4% paraformaldehyde (Sigma) and paraffin embedded for histology assessments. Histopathology was performed for tumors from $Trim27^{-/-}$ (n = 13) and $Trim27^{+/+}$ (n = 17) mice at week 22 after the initiation. Sections of tumors embedded into paraffin were stained using hematoxylin and eosin (Sigma). For Keratin 14 immunohistochemistry, antigen retrieval was performed in 10 mM citrate buffer pH 6.0 for 15 minutes in a microwave at 90°C followed by a 20-minute cool-down period at room temperature. Specimens were stained using rabbit polyclonal Keratin 14 antibody (dilution: 1/1000, PRB-155P; Covance, Leeds, UK) followed by horseradish peroxidase–coupled secondary antibody following standard procedures. The researcher who examined and scored the specimen was blinded to the genotype and the type of treatment administered to the mice.

For the generation of $Trim27^{-/-}Rb1^{+/-}$ mice, C57BL6 mice with disruption of the Rb1 locus through insertion of two iterative in-frame stop codons in exon 3 of the Rb1 gene (25) were paired with C57BL6 mice carrying the XP0484 Trim27 gene disruption. Genotyping was performed using genomic DNA from an ear-clip

biopsy with duplex PCR with primers Rbx3 (5′-AATTGCGGC CGCATCTGCATCTTTATCGC-3′) and RI3 (5′-CCCATGTT CGGTCCCTAG-3′) for the Rb1 wild-type allele, and primers Rbx3 and PGK3' (5′-GAAGAACGAGATCAGCAG-3′) for the Rb1 disrupted allele. $Trim27^{-/-}Rb^{+/+}$, $Trim27^{+/+}Rb^{+/+}$, $Trim27^{-/-}Rb^{+/-}$, and $Trim27^{+/+}Rb^{+/-}$ mice were observed during a period of 20 months for the appearance of thyroid and/or pituitary tumors. Mice that showed signs of distress or deterioration were killed under schedule 1 of the UK Animals (Scientific Procedures) Act of 1986. The pituitary gland and thyroid were examined for abnormalities along with all other internal organs. Surviving mice were killed at 20 months and examined. The researcher who examined the mice and recorded tumor incidence was blinded to the genotype of the mice. All in vivo experiments were approved by the UK Home Office and performed following the United Kingdom Coordinating Committee on Cancer Research Guidelines for the welfare and use of animals in cancer research.

Histochemical Detection of β-Geo and SA-β-Galactosidase Activity

Fresh whole-mount skin or tumors and sections of skin or tumors recently fresh frozen into OCT were fixed in 1% paraformaldehyde, 0.2% glutaraldehyde in PBS containing 2 mM magnesium chloride, 5 mM EGTA, and 0.02% Nonidet P-40 (NP-40) for 2 hours or 20 minutes, respectively, followed by three 30-minute rinses in PBS and 0.02% NP-40. For β-Geo detection, specimen were incubated in 5-bromo-4-chloro-indolyl-β-D-galactopyranoside (X-gal) solution (1 mg/mL X-gal, 5 mM potassium ferrocyanide, 5 mM potassium ferricyanide, 2 mM magnesium chloride, 0.01% sodium deoxycholate, and 0.02% NP-40 in PBS, pH 7.3) for 4 hours at 37°C. SA-β-gal was assayed essentially as described earlier. After the development of stain, samples were rinsed three times for 30 minutes each with PBS, 0.02% NP-40, mounted in 4',6-diamidino-2-phenylindole (DAPI)–containing mounting medium, and examined microscopically for evidence of staining.

Protein Analysis and Antibodies

Cell lysates were prepared in radio-immunoprecipitation assay buffer (PBS, 1% NP40, 0.5% sodium deoxycholate, 0.1% sodium dodecyl sulfate, and protease inhibitor cocktail; Roche). Protein samples were separated by sodium dodecyl sulfate–polyacrylamide gel electrophoresis (SDS-PAGE) and then transferred to polyvinylidene difluoride membrane of 0.45-μm pore size (GE Healthcare). Membranes were blocked with 5% nonfat dry milk in Tris-buffered saline (TBS; 25 mM Tris, 150 mM NaCl, 2 mM KCl, pH 7.4) with 0.1% Tween-20 (Sigma-Aldrich, Dorset, UK), referred to as TBST, at room temperature for 2 hours, followed by incubation at 4°C overnight with primary antibodies. Antibody used were rabbit polyclonal anti-$p19^{Arf}$ (dilution: 1/1000, ab80; Abcam, Cambridge, UK), mouse polyclonal anti-pan-Ras (dilution: 1/1000; Calbiochem, London, UK), mouse monoclonal anti-p21 (dilution: 1/1000, F5; Santa Cruz Biotechnology, Santa Cruz, CA), mouse monoclonal anti-β-actin (dilution: 1/1000, ACTN05; NeoMarkers, Surrey, UK), mouse monoclonal anti-p53 (dilution: 1/1000, 1C12; Cell Signaling, Hertfordshire, UK). Membranes were washed three times, 15 minutes each, with TBST before incubation at room temperature for 45 minutes with peroxidase-conjugated secondary antibodies (Dako UK Ltd, Cambridgeshire, UK) at 1:5000 dilution. All antibody dilutions were done in TBST with 1% nonfat dry milk. After washing the membranes with TBST three times, 15 minutes each, bound antibodies were visualized using Western Blotting Luminal Reagent (Santa Cruz Biotechnology).

Statistical Analysis

Data were analyzed using χ^2, Student's *t*, or log-rank test as appropriate for the analysis. Student's *t* test variants were applied as appropriate and are indicated, paired tests were used when possible, and heteroscedastic tests were applied when the samples compared showed unequal variance. Results were considered statistically significant when P was less than .05. Means and 95% confidence intervals are calculated where appropriate. Statistical analyses were performed using Office Excel (version 2007, Microsoft Office; licensed to University College London, London, UK) or GraphPad Prism (version 5; GraphPad Software Inc, La Jolla, CA). All statistical tests were two-sided. Experiments were powered to permit detection of 20% alteration in tumor incidence with 99% certainty at $P = .05$. Power calculations used the Cohen *d*.

Results

TRIM27 Expression in Human and Mouse Cancers

Previous studies have shown an increase in TRIM27 expression in specific cancers (5–7,26). We investigated whether enhanced TRIM27 expression may be detectable in other types of cancer and how widely this may be seen across cancer subtypes. We probed a commercial cancer-profiling array containing tumor cRNA (n = 261) alongside cRNA from paired normal tissue (n = 261) using the TRIM27-α coding region. Ubiquitin was used to control for loading-related signal inequalities. Analysis of normalized data across all samples revealed statistically significantly increased mean expression of TRIM27 in cancers vs normal tissues (TRIM27 expression relative to ubiquitin: cancers vs normal, mean = 0.59, 95% CI = 0.55 to 0.63 vs mean = 0.46, 95% CI = 0.43 to 0.49, $P < .001$) (Figure 1, A and Supplementary Figure 1, A, available online). TRIM27 expression was increased between two- and five-fold in individual cancers across all histological types, with others showing equal or decreased expression compared with matched normal tissue controls (Supplementary Figure 1, B–C, available online). Separation of data by tumor type indicates statistically significant increased TRIM27 expression in uterine (TRIM27 expression relative to ubiquitin: uterine cancers vs normal uterine tissues, mean = 0.74, 95% CI = 0.63 to 0.85 vs mean = 0.50, 95% CI = 0.44 to 0.56, $P < .001$, n = 42), colon (TRIM27 expression relative to ubiquitin: colon cancers vs normal colon tissues, mean = 0.50, 95% CI = 0.43 to 0.57 vs mean = 0.38, 95% CI = 0.30 to 0.46, $P < .01$, n = 35), rectal (TRIM27 expression relative to ubiquitin: rectal cancers vs normal rectal tissues, mean = 0.76, 95% CI = 0.51 to 1.0 vs mean = 0.43, 95% CI = 0.35 to 0.51, $P < .01$, n = 18), and lung (TRIM27 expression relative to ubiquitin: lung cancers vs normal lung tissues, mean = 0.61, 95% CI = 0.47 to 0.75 vs mean = 0.41, 95% CI = 0.35 to 0.47, $P < .01$, n = 21) cancers (Figure 1, B and Supplementary Figure 1, D, available online). Although TRIM27 expression was not statistically significantly

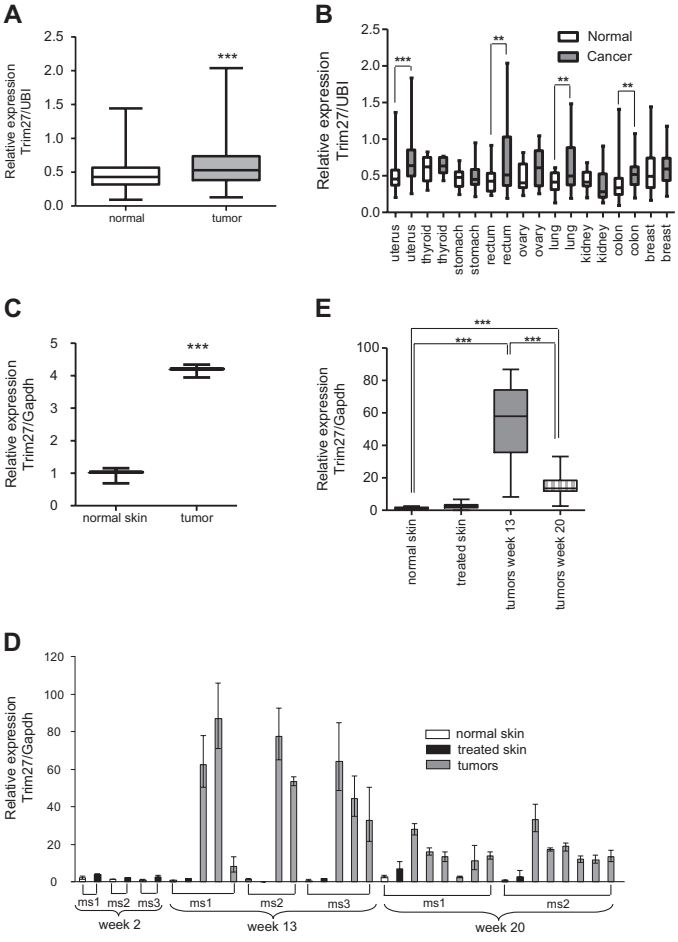

Figure 1. The tripartite motif family protein 27 (TRIM27) expression in human and mouse cancer. **A** and **B**) TRIM27 expression was assessed using Clontech cancer-profiling arrays containing 261 paired cancer and normal samples. Data were normalized to expression of Ubiquitin (UBI). **A**) A box plot of the relative expression of TRIM27 in human tumors and corresponding normal tissues is shown. ***$P < .001$ using heteroscedastic two-tailed Student's *t* test. **B**) Box plots depicting TRIM27 expression patterns for specific cancer types are shown. Paired two-tailed Student's *t* test was used to compare TRIM27 expression in cancer vs normal tissues **$P < .01$, ***$P < .001$. The number of tumors analyzed for each type are provided in Supplementary Figure 1 (available online). **C**) Box plot shows the expression of the Trim27 murine ortholog in chemically induced mouse skin tumors (n = 4) vs normal skin (n = 4) obtained 32 weeks after cancer initiation. Quantitative reverse transcription polymerase chain reaction analysis of Trim27 mRNA expression was done. Data were normalized to the expression of glyceraldehyde-3-phosphate dehydrogenase (Gapdh) and are presented as the relative quantitative score, with the mean Trim27 expression in corresponding skin set to 1. ***$P < .001$ using the paired two-tailed Student's *t* test. **D**) Trim27 transcript in chemically induced mouse skin, skin tumors, and normal skin in different mice (mouse 1 = ms1, mouse 2 = ms2, mouse 3 = ms3) obtained at week 2, 13, or 20 after tumor initiation. Data were normalized to the expression of Gapdh and are presented as the relative quantitative score, with the mean Trim27 expression in an arbitrarily chosen normal skin sample (ms3, week 2) set to 1. Mean expression levels are shown with corresponding 95% confidence intervals (**error bars**). Data from three replicates of one representative experiment are shown. **E**) Box plots showing the expression of the Trim27 murine ortholog in chemically induced mouse skin, skin tumors, and normal skin at 13 or 20 weeks after initiation are given. Data were normalized to the expression of Gapdh and are presented as the relative quantitative score with the mean Trim27 expression in an arbitrarily chosen normal skin sample set to 1. Normal skin (n = 8), tumors (n = 8) at week 13, tumors (n = 12) at week 20. Heteroscedastic two-tailed Student's *t* test was used to calculate *P*. ***$P < .001$. The box plots depict the median, and 25th to 75th percentiles with 5th to 95th percentiles are represented by the **whisker bars**.

(continued)

altered in breast cancer tissue, a subset of breast cancers showed enhanced expression when compared with paired normal tissue (Supplementary Figure 1, D, available online), potentially reflecting selective overexpression of TRIM27 in specific subgroups of disease, as was suggested in a recently published report (7).

To determine if Trim27 expression was increased in murine cancers, we examined murine tumors induced by exposure of the skin to the carcinogen DMBA followed by TPA treatment (27,28). Isolated tumor foci derived from individual mice 32 weeks after initiation were compared with paired samples of normal mouse skin using qRT-PCR. A statistically significant increase in Trim27 expression was observed among the murine cancers vs murine normal skin (Trim27 expression relative to Gapdh control: tumor vs normal skin, mean = 4.2, 95% CI = 3.97 to 4.43 vs mean = 0.96, 95% CI = 0.69 to 1.2, $P < .001$) (Figure 1, C), and was comparable to the degree by which Trim27 transcript levels were altered in the human cancer samples tested.

We further examined Trim27 expression in tumors and skin of mice at different stages of tumor development and compared expression between tumor foci that had developed in individual mice, which classically present with multifocal disease (21) (Figure 1, D and E). This revealed statistically significantly higher expression in tumors compared with normal skin at 13 weeks, which is a time when lesions are known to be hyperplastic and clonal yet mostly diploid (21) (Trim27 expression relative to Gapdh control: tumor vs normal skin, mean = 51.6, 95% CI = 34.2 to 69.0 vs mean = 1.34, 95% CI = 0.88 to 1.8, $P < .001$). Also, at 20 weeks, when anaplasia develops and lesions become progressively aneuploid (21), tumors again had statistically higher expression of Trim27 compared with normal skin (Trim27expression relative to Gapdh control: tumor vs normal skin, mean = 15.9, 95% CI = 11.4 to 20.4 vs mean = 1.34, 95% CI = 0.88 to 1.8, $P < .001$) (21). Levels of expression were remarkably high, 20- to 40-fold above normal skin, in early (13-week) lesions, as opposed to 10- to 20-fold in late (20-week) lesions. Furthermore, tumors without overt increase of Trim27 expression are found at both late and early times.

In contrast to the above, untreated and treated skin harvested 2 weeks following carcinogen exposure, a time at which tumors had not yet formed, showed comparable Trim27 expression. Likewise, when remotely located normal skin and tumor-adjacent skin harvested early (13 weeks) or late (20 weeks) following tumor initiation was compared, Trim27 expression was similar. Together, these results indicate that increased Trim27 expression accompanies and is exaggerated during early cancer development.

Furthermore, and paralleling the human data, inter-tumor heterogeneity exists in these murine cancers and is detectable at early (13 weeks) as well as late (20 weeks) times during cancer development, indicating that such heterogeneity more likely reflects the nature of the initiating event than cancer evolution during progression. Collectively, the data indicate increased

Figure 1 (continued).

TRIM27 expression across a considerable range of cancer types, including cancer in the mouse, and imply a role of TRIM27 overexpression in early cancers and cancer development.

Generation of Mice With Disruption of the Murine Trim27 Locus

To investigate if TRIM27 expression contributes to cancer development, we generated mice using mouse embryonic stem cells with a gene trap integration into the Trim27 locus. Long-range PCR combined with sequencing confirmed single-site integration into the first intron of the murine Trim27 gene (Figure 2, A). Positioning of the gene trap, which uses an En-2 splice acceptor site to direct fusion of the preceding exonic sequence to a bacterial β-galactosidase-(lacZ)-geneticin resistance hybrid gene, disrupts the murine Trim27 locus within the tripartite motif domain. Germline-modified chimeras, generated using these embryonic stem cells, gave rise to viable offspring that transmitted the trapped allele in a Mendelian fashion (Figure 2, B and Supplementary Table 1, available online), yielding normal sex ratios (Supplementary Table 1, available online). Mice with heterozygously or homozygously trapped Trim27 allele were indistinguishable from isogenic wild-type littermates, displaying no detectable differences in fitness, fertility, longevity, or behavior (Supplementary Table 1, available online, and data not shown).

We used qRT-PCR to confirm that the gene trap insertion affected the production of Trim27 transcript, using an intron 1-spanning probe set for Trim27 (Figure 2, C). Levels of Trim27 transcript in 14.5-day embryos were near detection limit in Trim27$^{-/-}$ embryos (Trim27 expression relative to Gapdh control, mean = 0.0055, 95% CI = 0.0051 to 0.0059) and reduced by approximately 50% in Trim27$^{+/-}$ (Trim27 expression relative to Gapdh control, mean = 0.53, 95% CI = 0.47 to 0.59) compared with Trim27$^{+/+}$ wild-type littermates (Trim27 expression relative to Gapdh control, mean = 1.0, 95% CI = 0.93 to 1.07) (Figure 2, D). A comparable reduction in signal was also seen with probe sets spanning Trim27 introns 2, 3, or 4 (Supplementary Figure 2, available

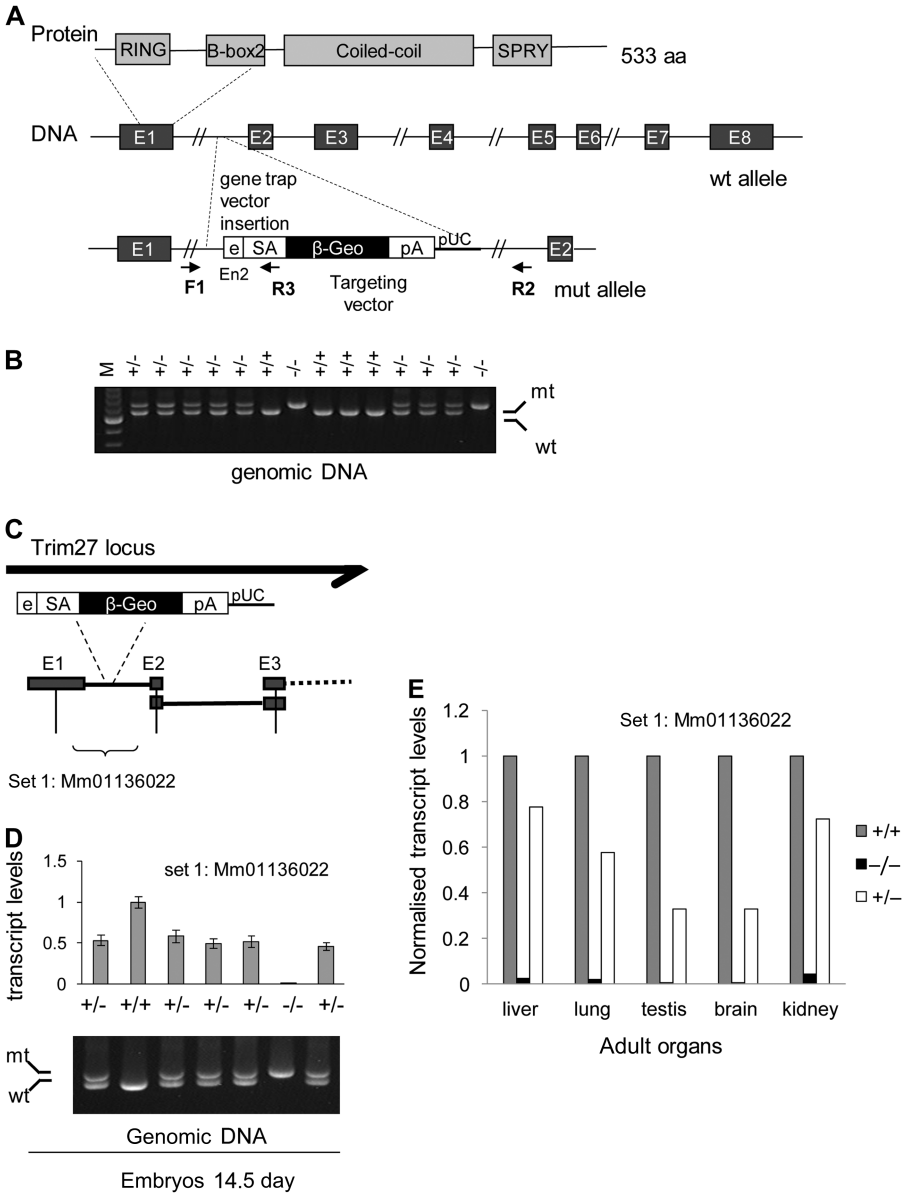

Figure 2. Gene trap–facilitated TRIM27 disruption. **A**) Schematic representation of gene trap insertion into the murine Trim27 locus. Insertion of the trap vector into intron 1 leads to splicing of the intron 1 splice donor into the trap encoded engrailed 2 (*En2*) intron1 splice acceptor (SA), generating an in-frame β-Geo fusion transcript followed by transcript termination. The locations of polymerase chain reaction (PCR) primers (F1, R3, R2) for distinguishing normal and trapped alleles are indicated. **B**) The viability of mice with the homozygously trapped Trim27 allele was determined. Multiplex PCR genotyping in the offspring of heterozygously trapped Trim27 mice was done. Wild type (wt) denotes the product from the normal, untrapped allele (660 bp) through priming with F1 and R2; mutant (mt) denotes the product from the trapped allele (731 bp) through priming with F1 and R3. **C**–**E**) The effect of gene trap insertion on Trim27 expression was determined. **C**) The position of primers for quantitative reverse transcription PCR analysis (qRT-PCR) is shown. **D**) Trim27 expression in 14.5-day embryos by qRT-PCR analysis. Data were normalized to the expression of glyceraldehyde-3-phosphate dehydrogenase (Gapdh) and are presented as the relative quantitative score, with the mean Trim27 expression in wild-type embryos set to 1. Mean expression levels and 95% confidence intervals (**error bars**) from three replicates of each representative embryo are shown. **E**) Trim27 expression in adult mouse organs was determined by qRT-PCR. Data represent the relative means for two individual mice normalized to the Gapdh control. Results for Trim27$^{+/+}$ organs were set to 1.

online) indicating that the gene trap insertion blocked generation of wild-type Trim27 transcript effectively and that no measurable intron skipping occurs that could give rise to C-terminal products from the trapped allele. To test if loss of Trim27 transcript production arises in adult mice, we looked at a panel of mouse organs. In line with prior published information (29), Trim27 transcript levels in adult organs were low compared with those seen in embryos with the exception of adult testis. In this organ (Trim27 expression relative to Gapdh control in testis, mean = 11.8, 95% CI = 10.7 to 13.0), a more than 10-fold higher expression of Trim27 was recorded than that seen in isogenic embryos (Trim27 expression relative to Gapdh control in embryos, mean = 1.0, 95% CI = 0.86 to 1.15) (Supplementary Figure 3, available online). Importantly, parallel analysis of organs from mice with hemizygously ($Trim27^{+/-}$) or homozygously ($Trim27^{-/-}$) trapped Trim27 revealed statistically significant lower levels of Trim27 transcript in the former and near absence in the latter across all organs tested (Figure 2, E) in comparison to $Trim27^{+/+}$ littermates (Trim27 expression relative to Gapdh control, $Trim27^{+/-}$ liver vs $Trim27^{-/-}$ liver vs $Trim27^{+/+}$ liver, mean = 0.77, 95% CI = 0.70 to 0.88 vs mean = 0.025, 95% CI = 0.018 to 0.033 vs mean = 1.0, 95% CI = 0.9 to 1.16; $Trim27^{+/-}$ lung vs $Trim27^{-/-}$ lung vs $Trim27^{+/+}$ lung, mean = 0.58, 95% CI = 0.48 to 0.7 vs mean = 0.017, 95% CI = 0.014 to 0.022 vs mean = 1.0, 95% CI = 0.87 to 1.13; $Trim27^{+/-}$ brain vs $Trim27^{-/-}$ brain vs $Trim27^{+/+}$ brain, mean = 0.33, 95% CI = 0.27 to 0.39 vs mean = 0.0044, 95% CI = 0.0028 to 0.0065 vs mean = 1.0, 95% CI = 0.85 to 1.17), consistent with observation in embryos. We concluded that the trap insertion robustly reduced the level of wild-type Trim27 transcript, giving rise to mice in which Trim27 is expressed at a substantially reduced level (Trim27 hypomorphs).

Skin Carcinogenesis in Mice with Trim27 Disruption

To assess whether the reduced production of Trim27 transcript may affect tumor formation, we examined tumor development in mice following DMBA/TPA exposure of their skin. Our previous analysis (Figure 1, C) showed increased expression of Trim27 at high frequency in such tumors. Tumors were detected in the carcinogen-treated mice 9–10 weeks after the initial application of DMBA and arose with similar latency in both $Trim27^{+/+}$ and $Trim27^{-/-}$ mice (Figure 3, A). However, a statistically significant percentage of $Trim27^{-/-}$ mice did not develop tumors. Among the $Trim27^{-/-}$ mice, eight (57.2 %) of 14 remained tumor free, whereas only one (7.7%) of 13 $Trim27^{+/+}$ mice was tumor free after 22 weeks, the time at which the experiment was terminated. The resistance to tumor development in $Trim27^{-/-}$ mice was also demonstrated by a reduced tumor burden in these mice. $Trim27^{-/-}$ tumor-bearing mice developed a smaller number of tumors compared with

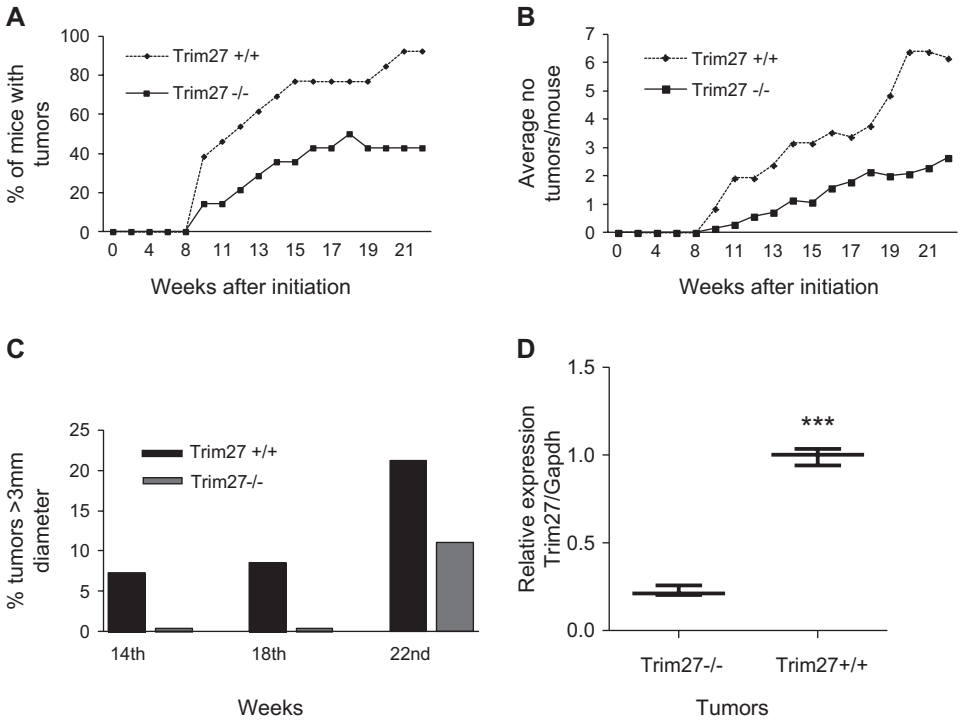

Figure 3. Skin carcinogenesis in wild-type ($Trim27^{+/+}$) and Trim27 mutant ($Trim27^{-/-}$) mice. **A–C**) Disease presentation in mice subjected to a two-stage chemical carcinogenesis protocol was studied, and statistical significance was measured by two-sided χ^2 tests. $^*P = .03$, $^{***}P < .001$. **A**) Tumor incidence in $Trim27^{+/+}$ (n = 13) and $Trim27^{-/-}$ (n = 14) mice and **B**) the average number of tumors per mouse among $Trim27^{+/+}$ (n = 6) and $Trim27^{-/-}$ (n = 2) were determined. **C**) The tumor burden for $Trim27^{+/+}$ and $Trim27^{-/-}$ mice (n = 13 and n = 14 respectively) was determined by caliper measurements of mouse skin tumors for the indicated times after tumor initiation. **D**) Box plot showing the expression of the Trim27 murine ortholog in chemically induced mouse skin $Trim27^{-/-}$ tumors (n = 4) vs $Trim27^{+/+}$ tumors (n = 4) obtained 32 weeks after tumor initiation. Quantitative reverse transcription polymerase chain reaction analysis of Trim27 mRNA expression was done, and the data were normalized to the expression of glyceraldehyde-3-phosphate dehydrogenase (Gapdh) and are presented as the relative quantitative score, with the mean Trim27 expression in $Trim27^{+/+}$ tumors set to 1. The median (**horizontal lines**), 25th to 75th percentiles (**boxes**), and 5th to 95th percentiles (**whiskers**) are indicated. $^{***}P < .001$ using heteroscedastic two-tailed Student's *t* test.

tumor-bearing Trim27$^{+/+}$ littermates (number of tumors per mouse: Trim27$^{-/-}$ vs Trim27$^{+/+}$, mean = 2.28, 95% CI = 0.57 to 3.99 vs mean = 6.38, 95% CI = 3.78 to 8.98, $P = .03$ as measured by the χ^2 test) (Figure 3, B and C), with tumors remaining small at week 22, only rarely reaching a size of 3 mm or larger (tumors >3 mm in diameter: Trim27$^{-/-}$ vs Trim27$^{+/+}$, 11.1% vs 21.3%, $P < .001$, χ^2 test) (Figure 3, C). At week 22, tumors were processed and stained with hematoxylin–eosin and for keratin 14. The morphology and histology of Trim27$^{-/-}$ and Trim27$^{+/+}$ tumors were identical. Evidence for stromal microinvasion was seen; yet these were detected regardless of genotype (Supplementary Table 2, available online).

Tumor development and tumor burden was also affected in Trim27$^{+/-}$ mice. Such mice displayed intermediate expressivity of tumor resistance, with tumor incidence and burden statistically significantly lower than observed in Trim27$^{+/+}$ mice (number of tumors per mouse: Trim27$^{+/-}$ vs Trim27$^{+/+}$, mean = 5.46, 95% CI = 3.28 to 7.64 vs mean = 9.76, 95% CI = 6.75 to 12.77, $P < .05$, χ^2 test), but higher than observed in Trim27$^{-/-}$ mice (number of tumors per mouse: Trim27$^{-/-}$ vs Trim27$^{+/+}$, mean = 2.46, 95% CI = 0.85 to 4.07 vs mean = 9.76, 95% CI = 6.75 to 12.77, $P < .001$, χ^2 test) at week 20 (Supplementary Figure 4, A–C, available online). Together, these results document that Trim27 transcript abundance critically influences tumor incidence as well as tumor expansion in the system studied.

To explore the distribution of Trim27 gene activation, histochemical detection was done for LacZ activity resulting from the β-Geo insertion that disrupted the Trim27 locus in Trim27$^{-/-}$ mice, which provides a reporter for locus activity (9). To obtain an initial overview, we performed full mount in situ staining using fixed whole tumors or skin. This revealed considerable β-Geo reporter activity in tumors from mice carrying the trapped allele but not in tumors from Trim27$^{+/+}$ mice (Supplementary Figure 4, E, available online). Staining was widespread across the tumor tissue with some variegation present in both early (week 14) and late cancers (week 20). Higher activity, relative to that at week 20, was generally observed at week 14. These observations are in line with results from qRT-PCR-based analysis indicating that more substantive Trim27 expression was present in early cancers (Figure 1, D and E). Histochemical detection using frozen sectioned material confirmed widespread β-Geo reactivity in tumor tissue but not in tumor-adjacent skin (Supplementary Figure 4, F, available online). Tumors showed specific staining in the epithelial layer of the lesions mostly involving the upper (squamous) layer of the epidermis (Supplementary Figure 4, G and H, available online) from which these cancers are thought to originate (21,30). Together, these results strongly support a view whereby ectopic activation of the Trim27 locus is localized to cancer tissue consistent with a tumor autonomous role of TRIM27.

Senescence Propensity in Embryo Fibroblasts With Trim27 Disruption

To investigate the mechanism by which Trim27 loss may prevent tumor development, we used MEFs isolated from 13.5-day-old mouse embryos, a cell type frequently used to study the mechanism of immortalization and oncogenic transformation ex vivo (31). Initially, we evaluated early passage 3 (P3) MEFs from Trim27$^{+/+}$ and Trim27$^{-/-}$ littermates under standard growth conditions. We found no difference in either proliferation capacity (live cell numbers on days 1 through 7 for Trim27$^{+/+}$ and Trim27$^{-/-}$ P3 MEFs were similar) (Figure 4, A) or the phenotypic appearance of these cells (Supplementary Figure 5, C, available online), suggesting that disruption of the Trim27 gene does not affect viability or proliferative capacity in early passaged MEFs. Explanted primary rodent fibroblasts have a finite life span in culture resulting in cessation of cell proliferation after a limited number of cell divisions (23,32–34). Cessation of population growth (crisis) is eventually overcome through outgrowth of rare variant cells with stochastically acquired mutations that serve to immortalize such primary cells in vitro.

To test whether Trim27 loss may affect the immortalization propensity of primary fibroblasts, we assessed the long-term proliferative capacity and life span of the various MEF lines using serial passage as prescribed by the 3T3 protocol (23). After a period of active growth (approximately 7–8 passages), the proliferative index of both Trim27$^{+/+}$ and Trim27$^{-/-}$ MEFs declined (Figure 4, B) alongside increased cell hypertrophy (Figure 4, C), an indicator of cellular senescence (35,36). However, although Trim27$^{+/+}$ MEFs escaped from this cessation of growth after about 20 days (7–10 passages), resuming and eventually adopting a stable rate of proliferation as typical for immortalized cultures, Trim27$^{-/-}$ MEFs underwent extended growth cessation with near absent proliferative activity for more than 50 days (approximately 20 passages) (Figure 4, B). This differential behavior of Trim27$^{+/+}$ and Trim27$^{-/-}$ MEFs was reproducibly seen in further littermate-paired MEF lines derived from independent litters (n = 3) (Supplementary Figure 5, A and B, available online). During the extended time of growth arrest observed for cultures of Trim27$^{-/-}$ MEFs, replicative senescence was indicated by an absence of mitotic activity, increase in the number of cells with hypertrophic morphology and positivity for the senescence marker enzyme SA-β-gal (percentage of SA-β-gal-positive cells: Trim27$^{+/+}$ MEFs vs Trim27$^{-/-}$ MEFs, mean = 14.2%, 95% CI = 11.1% to 17.4% vs mean = 53.3%, 95% CI = 48.7% to 57.9% at passage 17, $P < .001$) (24) (Figure 4, C and D, Supplementary Figure 5, D, available online). We concluded that loss of Trim27 decreased the incidence of spontaneous immortalization by increasing the propensity of primary mouse cells in culture to undergo senescence.

Effect of Trim27 Disruption on HRAS V12-Induced Senescence

Culture-associated replicative senescence in vitro is fueled by tissue culture inherent stresses including substratum stiffness and high oxygen pressure (37) and may have limited relevance in an organismal context. However, oncogenes including oncogenic versions of the RAS proto-oncogene family elicit senescence in cells and RAS oncogene–driven senescence is an established physiologically relevant mechanism of tumor suppression that limits transformation by oncogenic RAS mutants (35,38–43). Mutational activation of RAS is a prevalent oncogenic initiator event in chemically induced skin cancers in mice (27,44). Because Trim27 loss exaggerates replicative senescence, we investigated whether it also exaggerates senescence driven by RAS-activation. We introduced an activated RAS allele (HRAS V12) into Trim27$^{+/+}$ and Trim27$^{-/-}$

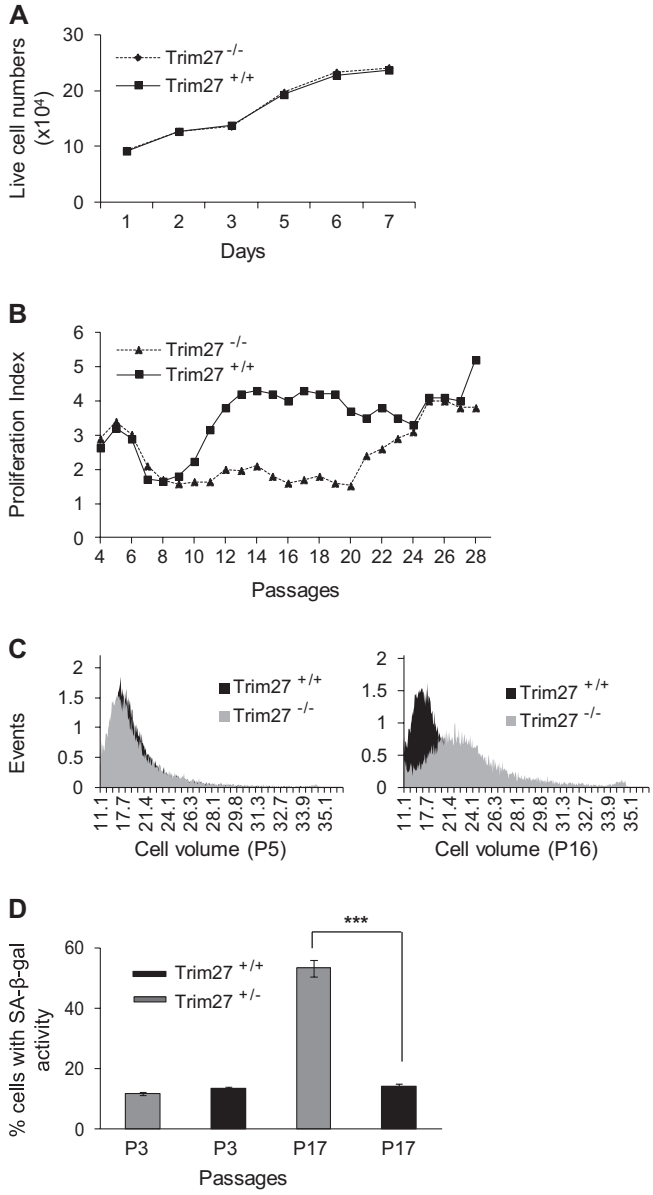

Figure 4. Growth properties of Trim27$^{-/-}$ mouse embryonic fibroblasts (MEFs) compared with litter-matched TRIM27$^{+/+}$ control MEFs. **A**) Growth of early-passage (passage 3) MEFs over 7 days was determined by counting the number of viable cells in a six-well plate by trypan blue exclusion. Results from one representative experiment are shown. Similar results were obtained when the experiment was repeated with three independent MEF preparations. **B**) The immortalization propensity in MEFs with Trim27 disruption. MEFs with indicated genotypes were seeded and passaged using the 3T3 protocol. The cumulative proliferation index calculated from the ratio between the number of cells plated and the number of cells harvested before further subculture is shown. Data points represent the mean count of cells harvested from three replicate dishes. The data are representative for three independent cell preparations (Supplementary Figure 5, available online). **C**) Cell volume in early- and late-passage MEFs was measured by a Scepter automated cell counter. Data are representative for three independent MEF preparations. **D**) The percentage of senescence-associated β-galactosidase (SA-β-gal)–positive cells was determined by counting SA-β-gal-positive cells in four eye fields each in three parallel dishes. Mean expression levels and 95% confidence intervals (**error bars**) of a representative experiment are shown. ***$P < .001$ using heteroscedastic two-tailed Student's *t* test.

MEFs using retroviral transduction. Consistent with previous observations (38), expression of HRAS V12 (Ras) in Trim27$^{+/+}$ MEFs resulted in senescence expressivity (Figure 5). However, and as seen with replicative senescence (Figure 4), the propensity for this response was considerably greater in Trim27$^{-/-}$ MEFs than in Trim27$^{+/+}$ MEFs, as indicated by increased attenuation of proliferation activity (Figure 5, A), enhanced appearance of cell hypertrophy, and an increase in the percentage of SA-β-gal positivity present in such cultures about 10 days following Ras transduction (percentage of SA-β-gal-positive cells: Trim27$^{+/+}$ MEFs + Ras vs Trim27$^{-/-}$ MEFs + Ras, mean = 24.0%, 95% CI = 19.9% to 28.1% vs mean = 37.3%, 95% CI = 32.2% to 42.4%, $P < .05$) (Figure 5, B). Similar results were obtained using paired Trim27$^{+/+}$ and Trim27$^{-/-}$

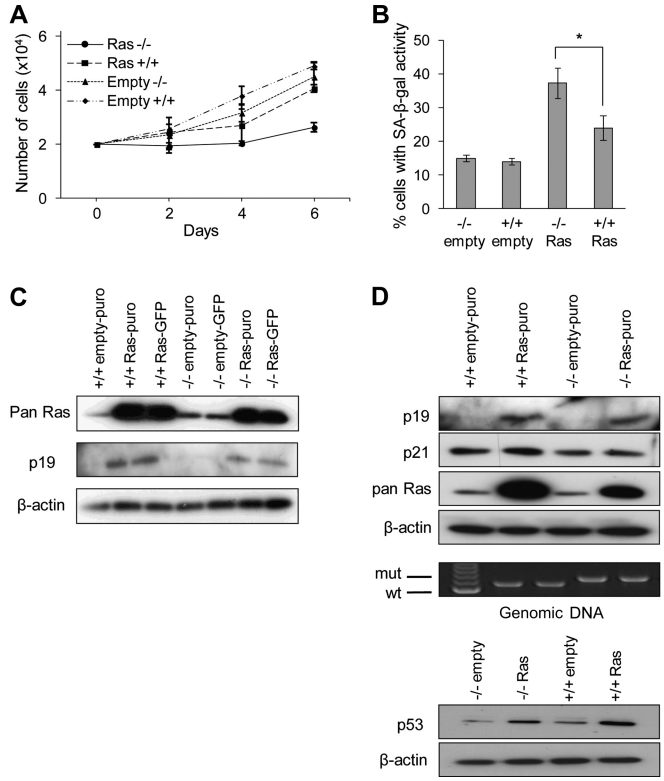

Figure 5. Trim27 loss exacerbates HRAS V12 oncogene-induced senescence. Passage 3 Trim27$^{+/+}$ and Trim27$^{-/-}$ mouse embryonic fibroblasts (MEFs) were infected with retrovirus encoding oncogenic HRAS V12 (Ras) or control (empty) vector and selected with puromycin. **A**) Growth curves depict the number of viable cells counted at the indicated times after infection and selection. The means and corresponding 95% confidence intervals (**error bars**) of three replicates within a representative experiment are shown. Three independent experiments were performed with similar results. **B**) The percentage of senescence-associated β-galactosidase (SA-β-gal)–positive Trim27$^{+/+}$ and Trim27$^{-/-}$ MEFs were calculated after retroviral infections. Mean expression levels and 95% confidence intervals (**error bars**) of a representative experiment were derived by counting SA-β-gal-positive cells in three eye fields each in three parallel dishes. *$P < .05$ using heteroscedastic two-tailed Student's *t* test. **C** and **D**) HRAS V12 oncogene expression and senescence signaling were assessed by immunoblot analysis of MEF cell lysates collected at day 7 after retroviral infection and selection by probing for Pan Ras, Arf (p19), p21CIP1/KIP1 (p21), and TP53 (p53). Detection of β-actin was used as a loading control. Data from two independent experiments are shown, involving HRAS V12 expressed from either the pBabe-Puro (-Puro) (**C**) or MSCV IRES GFP (-GFP) retroviral backbone (**C** and **D**) (Addgene).

MEF preparations from three different litters (not shown). The enhanced response of Trim27$^{-/-}$ cells was not because of exaggerated expression of the HRAS V12 protein in these cells nor the enhanced accumulation of the senescence drivers p19-ARF (p19), p21CIP1/KIP1 (p21), and TP53 (p53) (Figure 5, C and D), known to arise as a direct consequence of oncogenic HRAS V12 activation (22,35,45,46). This indicated that HRAS V12 signaling, including the induction of senescence-associated proteins, occurs normally in Trim27$^{-/-}$ cells. Hence, Trim27 loss exaggerates loss of proliferative capacity and cellular senescence in response to oncogenic stress.

To assess if senescence arises in Trim27$^{-/-}$ cancers in vivo and if senescence propensity in such cancers is enhanced in comparison to cancers arising in Trim27$^{+/+}$ backgrounds, we probed sections of mouse tumors for the presence of SA-β-gal activity (n = 3). This analysis revealed striking evidence for widespread senescence in Trim27$^{-/-}$ cancers that did not, however, extend to cancer adjacent skin nor was it seen in cancers with Trim27$^{+/+}$ background (Supplementary Figure 6, available online). These results are consistent with a view whereby enhanced senescence propensity is a feature arising in Trim27$^{-/-}$ backgrounds in conjunction with oncogenic transformation, further explaining the reduced disease incidence and progression seen in the Trim27$^{-/-}$ background.

Effect of Trim27 Loss on Senescence and Tumor Propensity in a Cancer Model With Rb1 Loss

A number of studies demonstrate the importance of the RB1 family proteins in executing the cellular senescence response (35,39,47,48). Moreover, we previously reported that TRIM27 overexpression attenuates RB1-driven senescence expressivity in human cells (19). To examine whether RB1 signaling plays a role in the increased senescence propensity seen in Trim27$^{-/-}$ MEFs, we infected early passage Trim27$^{-/-}$ and Trim27$^{+/+}$ MEFs from littermate embryos with either retrovirus encoding the human papillomavirus 16 E7 protein, which binds and inactivates RB family proteins, or a control (empty) virus. Following selection for virus uptake, we examined the proliferation behavior of such cultures using serial passage as scheduled by the 3T3 protocol (Figure 6, A). E7 expression effectively inhibited crisis and rescued proliferation in Trim27$^{-/-}$ cells, yielding proliferation capacity that was indistinguishable between Trim27$^{+/+}$ and Trim27$^{-/-}$ cells, hence providing evidence that RB1 family protein activity is required for the extended growth cessation in Trim27-deficient primary MEFs.

To further substantiate this view, we paired mice with an engineered defect in the mouse retinoblastoma protein–encoding locus (Rb1) (25) with mice carrying the Trim27 disruption. Whereas Trim27$^{-/-}$ MEFs with wild-type Rb1 expression developed extended proliferation inactivity, as previously observed, Trim27$^{-/-}$ MEFs with homozygous Rb1 defect adopted stable proliferation without signs of crisis or senescence, corroborating the notion that Rb1 function is critically required to establish the exaggerated senescence response seen in Trim27$^{-/-}$ MEFs (Figure 6, B).

Considering these observations, we asked whether Trim27 disruption affected cancer susceptibility in mice with hemizygous Rb1 loss (Rb$^{+/-}$). Such mice spontaneously develop pituitary and thyroid cancers with high penetrance through mechanisms of loss of heterozygosity (25). In contrast to mice with chemically induced skin cancers, where Trim27 disruption provides statistically significant cancer protection (Figure 3), Trim27$^{-/-}$ (n = 29) and Trim27$^{+/+}$ mice (n = 26) with hemizygous Rb1 loss showed identical cancer susceptibility, with similar time of onset, tumor frequency, and tumor spectrum (Trim27$^{-/-}$Rb$^{+/-}$ mice vs Trim27$^{+/+}$Rb$^{+/-}$ mice: median survival = 14.0 vs 13.0 months; difference = 1.0 month, 95% CI = 0.5 to 1.6 months, P = .14) (Figure 6, C and D). This is consistent with the hypothesis that cancer protection by Trim27 loss requires intact Rb signaling.

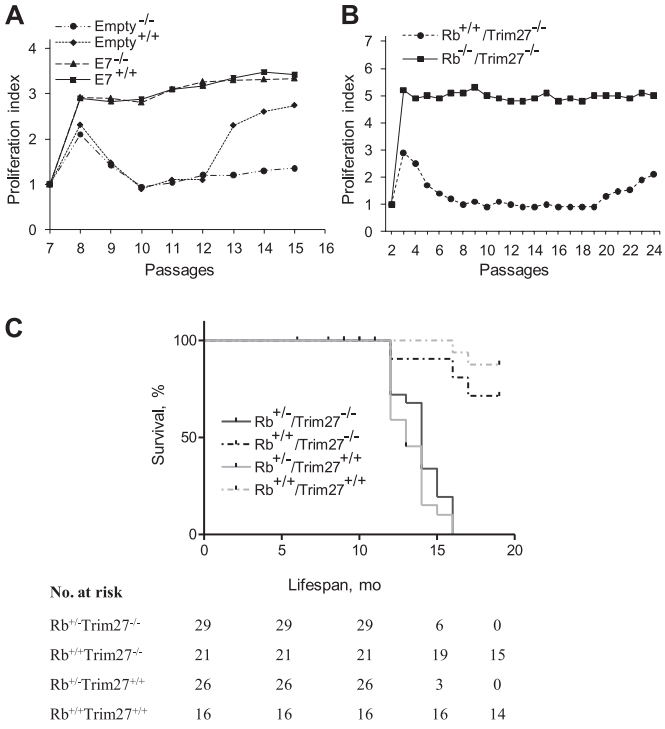

D

Mice	Pituitary tumors, %	Thyroid tumors, %
Rb$^{+/-}$Trim27$^{-/-}$	76.6	36.6
Rb$^{+/+}$Trim27$^{-/-}$	0	0
Rb$^{+/-}$Trim27$^{+/+}$	80.7	42.3
Rb$^{+/+}$Trim27$^{+/+}$	0	0

Figure 6. Senescence and tumor propensity in models with Rb1 loss. **A**) Senescence development in Trim27$^{-/-}$ backgrounds following papillomavirus E7 oncoprotein expression. Passage 3 mouse embryonic fibroblasts (MEFs) were infected with pBabe-puro-E7 or empty vector (Addgene) and selected with puromycin. Cells were cultured according to the 3T3 protocol. The data are representative for three independent cell preparations. **B**) Effect of Rb1 gene disruption on senescence arising in Trim27$^{-/-}$ backgrounds. MEFs with indicated genotypes were propagated in culture by following the 3T3 protocol. MEFs were derived from littermate embryos, generated by mating Trim27$^{-/-}$Rb$^{+/-}$ mice. Accumulated numbers of proliferation index were calculated as described before. Representative data of three independent MEF preparations are shown. **C**) Effect of Trim27 disruption on tumor susceptibility and survival in Rb1-deficient genetic background. Kaplan–Meier survival curves showing time to death in Rb$^{+/-}$Trim27$^{-/-}$ (n = 29), Rb$^{+/-}$Trim27$^{+/+}$ (n = 26), Rb$^{+/+}$Trim27$^{-/-}$ (n = 21), and Rb$^{+/+}$Trim27$^{+/+}$ (n = 16). A two-sided log-rank test was used to determine if Trim27 disruption affected survival in Rb$^{+/-}$Trim27$^{-/-}$ vs Rb$^{+/-}$Trim27$^{+/+}$ backgrounds. **D**) Tumor spectrum in mice with Trim27 disruption in Rb1-deficient genetic background was investigated, and the percentage of mice presenting with pituitary tumors and/or thyroid tumors was determined.

Discussion

We demonstrate here that TRIM27 expression is a contributing factor in the development of chemically induced skin cancer in mice. Previous publications have shown enhanced, and possibly aberrant, expression of TRIM27 transcript and protein in specific types of human cancer, including endometrial (6) and invasive breast cancer (7). Our data show that TRIM27 expression is also associated with cancers of the lung, colon, uterus, and prostate. Hence, TRIM27 overexpression may arise in an extended spectrum of sporadic human cancers. Our work provides strong evidence that TRIM27 overexpression has a putative role in these cancers by documenting that TRIM27 expression is a transformation promoting and hence a cancer-driving event.

We show that TRIM27 loss leads to exaggerated senescence in response to replicative as well as oncogene-associated stress. Senescence is recognized for its role in limiting oncogenic transformation, and hence exaggeration of this response in all likelihood explains the reduced tumor incidence in mice with compromised TRIM27 expression. A link between TRIM27 and senescence is suggested by our earlier work documenting reduced RB protein–driven senescence in human cells after enforced TRIM27 overexpression (19). The work shown here extends these observations and documents that RB1 signaling is a critical component of the exacerbated senescence response seen in Trim27-ablated mice.

Recent work has shown that TRIM27 overexpression confers resistance to oxidative stress, by decreasing the expression of thioredoxin binding protein-2 (26). Oxidative stress is thought to play a role in driving replicative as well as oncogene-associated senescence leading to p53 activation and the activation of stress activated kinases, culminating in enhanced p21CIP1/WAF1 expression (49,50). However, we have found no evidence for enhanced p53 activation or p21 expression in Trim27$^{-/-}$ MEFs nor did we observe enhanced expression of murine thioredoxin binding protein-2 in skin, tumors, or MEFs from Trim27$^{-/-}$ mice (data not shown), suggesting that our observations may be unrelated to the transcriptional regulation of this gene and the resultant enhanced oxidative stress.

To generate mice with impaired TRIM27 expression, we used murine embryonic stem cells in which the TRIM27 locus was modified through insertion of a gene trap that leads to greater than 80% reduction in TRIM27 transcript expression in all tissues tested. Apart from considerable cancer resistance, mice with trapped TRIM27 locus are normal without any evident deficiencies, suggesting that substantial loss of TRIM27 gene function is possible without overt toxic effects. The demonstrated reduction of cancer incidence and progression in mice with TRIM27 loss, and the documentation of enhanced TRIM27 expression in a wide spectrum of human cancers, indicates that TRIM27 inhibition is a potential pharmacological target for therapy and/or chemoprevention of cancer.

The presented study has several limitations, one being that a murine skin cancer model driven by carcinogen exposure is used rather than a genetically defined model of a human cancer type where TRIM27 is found to be overexpressed. This currently limits the ability to predict whether cancer reduction extends to these human cancers. The study design investigating the effect of TRIM27 loss in chemically induced skin cancer was led by experimental observations showing TRIM27 expression to be enhanced in these murine cancers, suggesting that this cancer type is a relevant model for studying the role of the expression change. While the cancer-initiating driver alteration (K- or H-Ras), the cell of origin, and the genetics and biology of progression have been characterized in detail in the model used (21), chemically induced cancers do not rely on engineered and preexisting genetic alterations. In this, they may more closely resemble the natural evolution of sporadically emerging human cancers than do models reliant on specific genetic changes. However, because the genetics of chemically induced cancers is likely to be heterogeneous, the current work does not allow prediction if TRIM27 overexpression generally limits cancer development or does so only in the context of specific cancer-driving genetic event. Justified by the results reported here, it will be important in future work to test for modification of cancer susceptibility in murine models of human cancers that show TRIM27 locus activation and in the context of genetically defined murine models of cancer development.

A further limitation is that currently no data are available as to the spatial distribution of TRIM27 expression in human or murine cancer tissue. To provide a preliminary view, we monitored TRIM27 locus activation through histochemical detection of the β-Geo reporter gene that has been inserted and is transcribed in place of the TRIM27 encoding sequence in the Trim27-trapped mouse model. To confirm and extend these results, it will be important in future work to develop antibodies suitable for histochemical detection of the TRIM27 protein in murine and human cancer tissue.

An important question that currently remains unanswered is whether TRIM27 loss is required in late cancer or merely plays a role in early cancers and during cancer initiation. Although our findings document the requirement for TRIM27 expression during tumor development, further investigations as to the need for TRIM27 during cancer progression are clearly warranted.

References

1. Hanahan D, Weinberg RA. Hallmarks of cancer: the next generation. *Cell.* 2011;144(5):646–674.
2. Hanahan D, Weinberg RA. The hallmarks of cancer. *Cell.* 2000; 100(1):57–70.
3. Takahashi M, Ritz J, Cooper GM. Activation of a novel human transforming gene, ret, by DNA rearrangement. *Cell.* 1985;42(2):581–588.
4. Hasegawa N, Iwashita T, Asai N, et al. A RING finger motif regulates transforming activity of the rfp/ret fusion gene. *Biochem Biophys Res Commun.* 1996;225(2):627–631.
5. Tezel G, Nagasaka T, Shimono Y, et al. Differential expression of RET finger protein in testicular germ cell tumors. *Pathol Int.* 2002;52(10): 623–627.
6. Tsukamoto H, Kato T, Enomoto A, et al. Expression of Ret finger protein correlates with outcomes in endometrial cancer. *Cancer Sci.* 2009;100(10): 1895–1901.
7. Tezel GG, Uner A, Yildiz I, et al. RET finger protein expression in invasive breast carcinoma: relationship between RFP and ErbB2 expression. *Pathol Res Pract.* 2009;205(6):403–408.
8. McNab FW, Rajsbaum R, Stoye JP, et al. Tripartite-motif proteins and innate immune regulation. *Curr Opin Immunol.* 2011;23(1):46–56.
9. Skarnes WC, von Melchner H, Wurst W, et al. A public gene trap resource for mouse functional genomics. *Nat Genet.* 2004;36(6):543–544.

10. Shieh PB, Kudryashova E, Spencer MJ. Limb-girdle muscular dystrophy 2H and the role of TRIM32. *Handb Clin Neurol.* 2011;101:125–133.
11. Munir M. TRIM proteins: another class of viral victims. *Sci Signal.* 2010;3(118):jc2.
12. Hatakeyama S. TRIM proteins and cancer. *Nat Rev Cancer.* 2011;11(11): 792–804.
13. Chu Y, Yang X. SUMO E3 ligase activity of TRIM proteins. *Oncogene.* 2011;30(9):1108–1116.
14. Matsuura T, Shimono Y, Kawai K, et al. PIAS proteins are involved in the SUMO-1 modification, intracellular translocation and transcriptional repressive activity of RET finger protein. *Exp Cell Res.* 2005;308(1):65–77.
15. Meroni G, Diez-Roux G. TRIM/RBCC, a novel class of 'single protein RING finger' E3 ubiquitin ligases. *Bioessays.* 2005;27(11):1147–1157.
16. Gillot I, Matthews C, Puel D, et al. Ret finger protein: an E3 ubiquitin ligase juxtaposed to the XY body in meiosis. *Int J Cell Biol.* 2009;2009:524858.
17. Napolitano LM, Jaffray EG, Hay RT, et al. Functional interactions between ubiquitin E2 enzymes and TRIM proteins. *Biochem J.* 2011;434(2): 309–319.
18. Shimono Y, Murakami H, Hasegawa Y, et al. RET finger protein is a transcriptional repressor and interacts with enhancer of polycomb that has dual transcriptional functions. *J Biol Chem.* 2000;275(50):39411–39419.
19. Krutzfeldt M, Ellis M, Weekes DB, et al. Selective ablation of retinoblastoma protein function by the RET finger protein. *Mol Cel.l.* 2005;18(2):213–224.
20. Zha J, Han KJ, Xu LG, et al. The Ret finger protein inhibits signaling mediated by the noncanonical and canonical IkappaB kinase family members. *J Immunol.* 2006;176(2):1072–1080.
21. Abel EL, Angel JM, Kiguchi K, et al. Multi-stage chemical carcinogenesis in mouse skin: fundamentals and applications. *Nat Protoc.* 2009;4(9):1350–1362.
22. Alani RM, Young AZ, Shifflett CB. Id1 regulation of cellular senescence through transcriptional repression of p16/Ink4a. *Proc Natl Acad Sci U S A.* 2001;98(14):7812–7816.
23. Todaro GJ, Green H. Quantitative studies of the growth of mouse embryo cells in culture and their development into established lines. *J Cell Biol.* 1963;17(2):299–313.
24. Dimri GP, Lee X, Basile G, et al. A biomarker that identifies senescent human cells in culture and in aging skin in vivo. *Proc Natl Acad Sci U S A.* 1995;92(20):9363–9367.
25. Jacks T, Fazeli A, Schmitt EM, et al. Effects of an Rb mutation in the mouse. *Nature.* 1992;359(6393):295–300.
26. Kato T, Shimono Y, Hasegawa M, et al. Characterization of the HDAC1 complex that regulates the sensitivity of cancer cells to oxidative stress. *Cancer Res.* 2009;69(8):3597–3604.
27. Kemp CJ. Multistep skin cancer in mice as a model to study the evolution of cancer cells. *Semin Cancer Biol.* 2005;15(6):460–473.
28. Boutwell RK, Verma AK, Ashendel CL, et al. Mouse skin: a useful model system for studying the mechanism of chemical carcinogenesis. *Carcinog Compr Surv.* 1982;7:1–12.
29. Cao T, Shannon M, Handel MA, et al. Mouse ret finger protein (rfp) proto-oncogene is expressed at specific stages of mouse spermatogenesis. *Dev Genet.* 1996;19(4):309–320.
30. Lapouge G, Youssef KK, Vokaer B, et al. Identifying the cellular origin of squamous skin tumors. *Proc Natl Acad Sci U S A.* 2011;108(18):7431–7436.
31. Sun H, Taneja R. Analysis of transformation and tumorigenicity using mouse embryonic fibroblast cells. *Methods Mol Biol.* 2007;383:303–310.
32. Hayflick L, Moorhead PS. The serial cultivation of human diploid cell strains. *Exp Cell Res.* 1961;25:585–621.
33. Sherr CJ, DePinho RA. Cellular senescence: mitotic clock or culture shock? *Cell.* 2000;102(4):407–410.
34. Zhang H. Molecular signaling and genetic pathways of senescence: its role in tumorigenesis and aging. *J Cell Physiol.* 2007;210(3):567–574.
35. Ben-Porath I, Weinberg RA. The signals and pathways activating cellular senescence. *Int J Biochem Cell Biol.* 2005;37(5):961–976.
36. Blagosklonny MV. Cell senescence: hypertrophic arrest beyond the restriction point. *J Cell Physiol.* 2006;209(3):592–597.
37. Cristofalo VJ, Lorenzini A, Allen RG, et al. Replicative senescence: a critical review. *Mech Ageing Dev.* 2004;125(10–11):827–848.
38. Serrano M, Lin AW, McCurrach ME, et al. Oncogenic ras provokes premature cell senescence associated with accumulation of p53 and p16INK4a. *Cell.* 1997;88(5):593–602.
39. Weinberg RA. The cat and mouse games that genes, viruses, and cells play. *Cell.* 1997;88(5):573–575.
40. Peeper DS, Dannenberg JH, Douma S, et al. Escape from premature senescence is not sufficient for oncogenic transformation by Ras. *Nat Cell Biol.* 2001;3(2):198–203.
41. Collado M, Gil J, Efeyan A, et al. Tumour biology: senescence in premalignant tumours. *Nature.* 2005;436(7051):642.
42. Dimri GP. What has senescence got to do with cancer? *Cancer Cell.* 2005;7(6):505–512.
43. Chandeck C, Mooi WJ. Oncogene-induced cellular senescence. *Adv Anat Pathol.* 2010;17(1):42–48.
44. Quintanilla M, Brown K, Ramsden M, et al. Carcinogen-specific mutation and amplification of Ha-ras during mouse skin carcinogenesis. *Nature.* 1986;322(6074):78–80.
45. Palmero I, Pantoja C, Serrano M. p19ARF links the tumour suppressor p53 to Ras. *Nature.* 1998;395(6698):125–126.
46. Shay JW, Roninson IB. Hallmarks of senescence in carcinogenesis and cancer therapy. *Oncogene.* 2004;23(16):2919–2933.
47. Takahashi A, Ohtani N, Yamakoshi K, et al. Mitogenic signalling and the p16INK4a-Rb pathway cooperate to enforce irreversible cellular senescence. *Nat Cell Biol.* 2006;8(11):1291–1297.
48. Chicas A, Wang X, Zhang C, et al. Dissecting the unique role of the retinoblastoma tumor suppressor during cellular senescence. *Cancer Cell.* 2010;17(4):376–387.
49. Campisi J. Senescent cells, tumor suppression, and organismal aging: good citizens, bad neighbors. *Cell.* 2005;120(4):513–522.
50. Lu T, Finkel T. Free radicals and senescence. *Exp Cell Res.* 2008;314(9): 1918–1922.

Funding

The work reported was supported by grants from Cancer Research UK (C107/A3096, C107/A10437, and C107/10433).

Notes

We thank Dr Fredrik Wallberg, The Institute of Cancer Research, for assistance with fluorescence-activated cell sorting. We thank Ian Rosewell, Cancer Research UK London Research Institute, for assistance with embryonic stem cell propagation and blastocyst injection.

Affiliations of authors: UCL Cancer Institute, University College London, London, UK (GZ, SM); Formerly of The Institute of Cancer Research, Section for Cell and Molecular Biology, Chester Beatty Laboratories, London, UK (GZ, CB, HL, DB, GT, SM); Technology Transfer CIBER of Respiratory Diseases (CIBERES), Barcelona, Spain (CB); Institute of Ophthalmology, University College London, London, UK (HL); Knight Cancer Institute, Oregon Health and Science University, Portland, OR (GT).